HEALTH AND MEDICINE

Dissolved oxygen from microalgae-gel patch promotes chronic wound healing in diabetes

Huanhuan Chen[1]*, Yuhao Cheng[1]*, Jingrun Tian[1], Peizheng Yang[1], Xuerao Zhang[1], Yunhao Chen[1], Yiqiao Hu[1,2†], Jinhui Wu[1,2,3†]

Chronic wounds in diabetes undergo a lifetime risk of developing into diabetic foot ulcers. Oxygen is crucial to wound healing by regulating cell proliferation, migration, and neovascularization. However, current oxygen therapies, including hyperbaric oxygen (HBO) and topical gaseous oxygen (TGO), mainly employ gaseous oxygen delivery, which is much less effective in penetrating the skin. Here, we introduce an oxygen-producing patch, made of living microalgae hydrogel, which can produce dissolved oxygen. The superior performance of the patch that results from its dissolved oxygen delivery is >100-fold much more efficient than TGO penetrating the skin. Further experiments indicate that the patch could promote cell proliferation, migration, and tube formation in vitro, and improve chronic wound healing and the survival of skin grafts in diabetic mice. We believe that the microalgae-gel patch can provide continuous dissolved oxygen to improve chronic wound healing.

INTRODUCTION

Diabetes affects 425 million people, and its prevalence will increase to 629 million by 2045 worldwide (1). At present, as many as 25% of diabetics face a lifetime risk of chronic nonhealing wounds, such as diabetic foot ulcers (DFUs), putting patients at risk of amputation; at least 68% of these individuals will die within 5 years (2). Researchers have demonstrated that delayed healing in diabetic chronic wounds is a result of damaged neovascularization in response to hypoxia (3–5). High-glucose exposure interferes with hypoxia-inducible factor–1α (HIF-1α) stability by affecting its rapid hydroxylation and degradation following translation. This change results in a failure of the diabetic wound to up-regulate vascular endothelial growth factor (VEGF) in response to soft tissue ischemia, which leads to impaired angiogenesis and wound healing (4–6). Therefore, reduction of hypoxia in treatment of chronic wounds is an urgent clinical problem in diabetes.

However, existing methods do not easily sustain or deliver sufficient oxygen to the wounds due to their reliance on gaseous oxygen as the oxygen source. For example, hyperbaric oxygen (HBO) inhalation cannot prevent local ischemia in the wound; topical gaseous oxygen (TGO) therapy is hampered by the limited penetration of external gas to the tissues (7–9). In practice, HBO and TGO have been shown to be effective for some cases of delayed wound healing (8, 10, 11), but are not always found to bring statistically significant improvements, owing to their limited efficacy (12–14). Besides, oxygen level can only be temporarily elevated for 1 to 2 hours during TGO/HBO treatment, returning to baseline levels within several minutes once the patient is removed from the chamber (7). Furthermore, the failure of oxygen supply also makes it unsuitable for other treatments to heal chronic wounds such as transplantation and growth factor therapies. Therefore, local delivery of dissolved oxygen is the most effective way to improve the healing of diabetic chronic wounds.

Here, we develop a patch-like wound dressing to cover the wound and establish a local moist HBO atmosphere for dissolved oxygen delivery. The patch is filled with gel beads containing active *Synechococcus elongatus* (*S. elongatus*) PCC7942, a unicellular cyanobacterium that represents a preeminent model for the study of circadian rhythms (15, 16). Topical dissolved oxygen (TDO) has been reported to penetrate through >700 μm of human skin, while TGO penetrates only 300 μm of dermis (17–21). Therefore, delivery of TDO is the most effective way to improve the diabetic chronic wounds. On the basis of these characteristics, we hypothesized that *S. elongatus* PCC7942 could be used in diabetic chronic wounds with the essential dissolved oxygen for tissue repair. Specifically, we found that algae-gel wound dressing increases wound oxygenation, fibroblast proliferation, and angiogenesis. Furthermore, this patch is nontoxic and does not elicit an immune response, which would serve as a new generation of medical therapeutics for DFU treatment.

RESULTS

O$_2$ liberation of PCC7942

We designed the patch dressing, named alga-gel patch (AGP), that can simply cover the wound and deliver dissolved oxygen into wound bed (Fig. 1A). Hydrogel beads 1 mm in diameter containing living microalgae were filled in the patch, which can consume carbonates (CO_3^{2-} and HCO_3^-) added in advance to produce O_2 and CO_2 through respiration and photosynthesis. Hydrophilic polytetrafluoroethylene (PTFE) membrane with a 0.22-μm aperture was used as the lining of AGP, to allow the bidirectional permeations of clean gases and water with bacteria filtration performances. When affixed to the wound, a sealing system is formed between the dressing and the wound owing to the impermeable polyurethane film used as the back liner of AGP (Fig. 1, B and C). We assume that the carbon dioxide, oxygen, and humidity of the wound can be sufficiently raised and regulated by AGP, to repair tissue in a full-time, aerobic, and wet healing manner.

We first confirmed the activity of the gel beads by giving red light irradiation and monitoring the dissolved oxygen using a microelectrode. Under sufficient light, the dissolved oxygen concentration of the PCC7942 solution increased gradually from 0 to over 600 μM

[1]State Key Laboratory of Pharmaceutical Biotechnology, Medical School and School of Life Sciences, Nanjing University, Nanjing 210093, China. [2]Jiangsu Provincial Key Laboratory for Nano Technology, Nanjing University, Nanjing 210093, China. [3]Chemistry and Biomedicine Innovation Center, Nanjing University, Nanjing 210023, China.
*These authors contributed equally to this work.
†Corresponding author. Email: huyiqiao@nju.edu.cn (Y.H.); wuj@nju.edu.cn (J.W.)
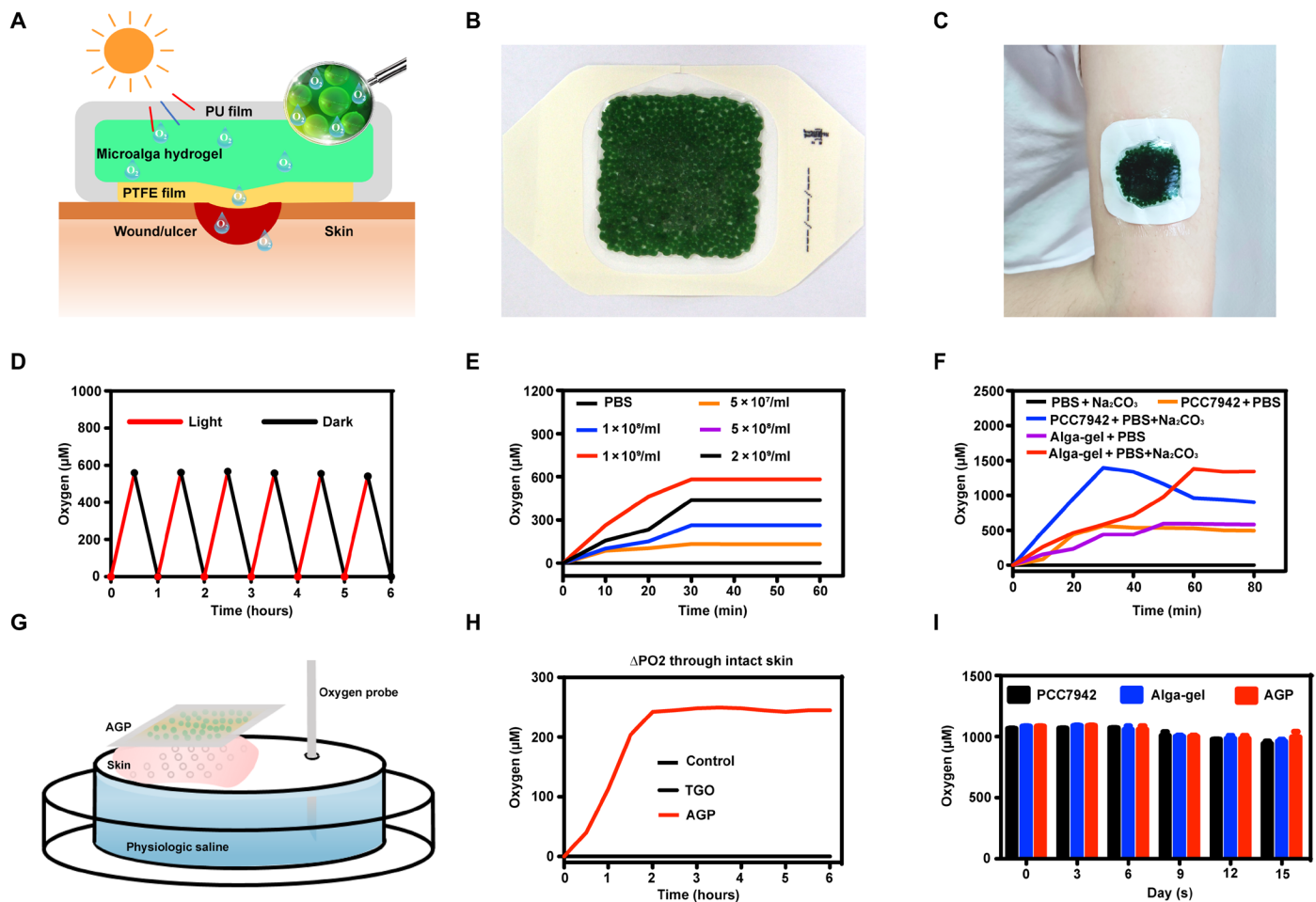
Fig. 1. AGP released dissolved oxygen through the intact skin. (**A**) Schematic illustration of microalga-hydrogel patch (AGP) preparation through polyurethane film and polytetrafluoroethylene membrane to perform the light response dissolved oxygen release for chronic wound. (**B**) Images of the AGP. (**C**) Photograph of the AGP sticking on the arm. (**D**) Comparison of releasing dissolved oxygen of alga-gel under light or dark conditions. (**E**) Comparison of releasing dissolved oxygen of PCC7942 with different concentrations. (**F**) Comparison of releasing dissolved oxygen between the PCC7942 solution and alga-gel (1×10^9 cells/ml) supplement with or without 500 µM Na_2CO_3. (**G**) Diagram of apparatus for measuring delivery of dissolved oxygen. (**H**) Transfer of dissolved oxygen through mice intact skin into saline at 37°C. (**I**) Comparison of releasing dissolved oxygen during the storage of PCC7942 solution, alga-gel beads, and AGP (1×10^9 cells/ml) at days 0, 5, 10, and 15. Photo credit (B and C): Huanhuan Chen (Medical School and School of Life Sciences, Nanjing University).

in 30 min; under dark conditions, the dissolved oxygen decreased from 600 to more than 0 µM in 30 min (Fig. 1D). These results demonstrated that the microalgae in the PCC7942 have complete activity and can carry out photosynthesis and respiration. The oxygen production rate was positively correlated with the concentration of PCC7942 in a certain range, and the optimum concentration was 1×10^9/ml (Fig. 1E).

As autotrophic organisms, PCC7942 can uptake inorganic carbon (CO_2, CO_3^{2-}, and HCO_3^-) to release O_2 by photosynthesis (fig. S1A). Hence, we hypothesized that additional carbonates in PCC7942 can contribute to the O_2 productivity. To verify this, different concentrations of Na_2CO_3 were added into PCC7942 (fig. S1B). PCC7942 solution was sealed, and the upper limit of dissolved oxygen generation in 0, 125, 250, and 500 µM Na_2CO_3 was gradually increased from about 480 to 1400 µM, suggesting that the concentration of inorganic carbon can enhance the performance of PCC7942. In addition, we did not find obvious differences between immobilized alga-gel solution and free PCC7942 solution under the same concentrations (Fig. 1F).

O₂ skin penetration test of AGP

Initial experiments were performed to determine the transfer kinetics of oxygen from the AGP to saline without introducing the variable of interposed human skin in the system. Dissolved oxygen measurement without percutaneous process began to rise immediately with AGP and TGO (*13*), and the maximum change in oxygen concentration reached 550 µM for the AGP device at 40 min and 558 µM for TGO at 30 min (fig. S1C). There was no difference in peak oxygen level between AGP and TGO.

Next, the diffusion of oxygen from devices through interposed viable mice skin (300 to 400 µm) in the apparatus was measured (Fig. 1G). The AGP device was able to stably and continuously deliver dissolved oxygen up to 240 µM under light conditions, but there was no diffusion of oxygen in the TGO device (Fig. 1H). By quantifying the area under the curve (Fig. 1H), we find that the dissolved oxygen delivery of AGP is >100-fold much more efficient than TGO penetrating the skin. It turned out that the epidermis provided a significant barrier to diffusion of oxygen due to the lack of blood vessels. However, water

can penetrate the stratum corneum and enter the epidermis through sweat ducts and hair follicles (*13*, *19*). Our data confirm that topically applied dissolved oxygen penetrates mouse skin at a faster rate and to a greater depth than TGO, which was consistent with Roe *et al.*'s report (*13*).

Stability studies of AGP

We measured the oxygen production of PCC7942 (fig. S1D), alga-gel (fig. S1E), and AGP (fig. S1F) stored for 15 days at 4°C under light conditions. Dissolved oxygen of each group was able to reach about 1000 μM, and there were no differences among PCC7942, alga-gel, and AGP for 15 days (Fig. 1I). Therefore, we confirmed that AGP has a storage stability fixed to satisfy therapeutic needs.

Alga-gel promoted wound healing and angiogenesis in vitro

Wound healing consists of multiple cells participating simultaneously, such as fibroblast proliferation, keratinocyte migration, and endothelial cell differentiation (*22*); thus, the effect of alga-gel on several cells including human umbilical vein endothelial cells (HUVECs), human immortalized keratinocytes (HaCaTs), and human skin fibroblasts (HSFs) was verified.

The relationship between hypoxia and hyperglycemia was first evaluated (*23*), we found that exposure with 33 mM glucose and 1% O_2 did result in cell hypoxia with overexpression of HIF-1α (Fig. 2, B and C, and fig. S2, A and D). Then, we have evaluated that alga-gel could markedly reverse cell hypoxia and a 78.3% decrease of HIF-1α in HSFs (Fig. 2, B and C). On this basis, the effect of alga-gel for HSF proliferation was further examined, and the proliferation rate of HSFs with alga-gel in the light was significantly higher than that of the high-glucose group and even the TGO group (Fig. 2, D and E), indicating that the dissolved oxygen released from PCC7942 has notable granulation tissue potential by HSF proliferation.

Ideally, the scratch wound healing of keratinocytes is central in re-epithelialization processes during chronic wound healing (*22*). We therefore investigated the effect of dissolved oxygen from alga-gel on hypoxia-induced HaCaT. The migration of HaCaT was significantly inhibited by hypoxia and high glucose, and stimulation with alga-gel in the light resulted in increasing migration of HaCaT (Fig. 2, F and G). Significant difference was observed in cell migration between alga-gel and TGO ($P < 0.05$), which manifested that the dissolved oxygen released from PCC7942 could promote chronic wound healing by promoting epithelialization.

Endothelial cells are essential cells for blood vessels and play an important role in vascularization (*24*). We conducted scratch wound healing, cell migration, and tube formation assays by using fluorescence microscopy and transmission electron microscopy. At first, we performed the scratch assay, an experiment for measuring endothelial cell proliferation/migration in vitro, which is a critical step of
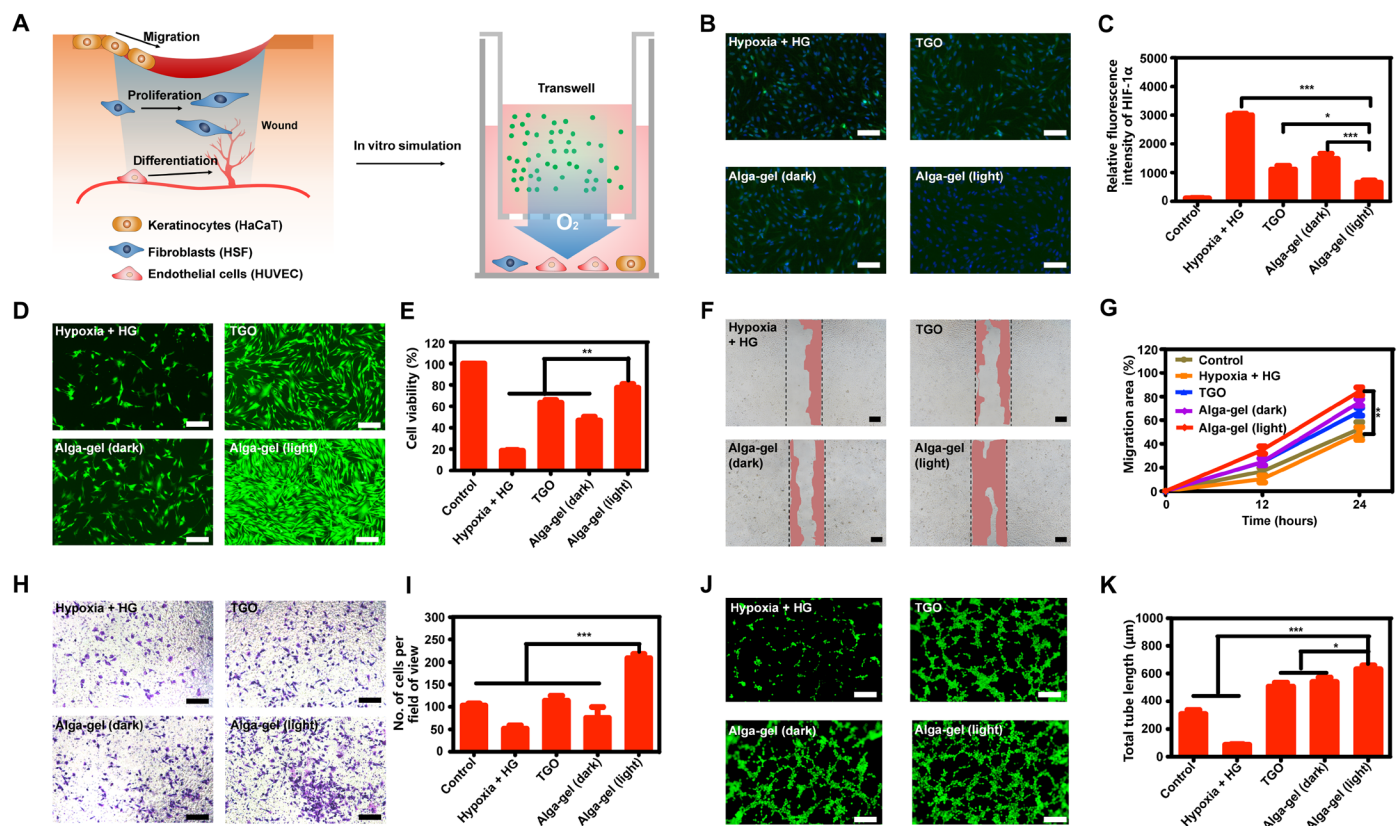

Fig. 2. Alga-gel activates cells against hypoxia and high glucose in vitro. (**A**) Illustration of the wound-healing process and design scheme with alga-gel. (**B** and **C**) Alga-gel reduced HIF-1α on high glucose–induced HSF ($n = 3$). Scale bars, 200 μm. (**D** and **E**) HSF cell proliferation with 33 mM glucose and 6 hours of hypoxia in different groups ($n = 3$). Scale bars, 200 μm. (**F** and **G**) Representative images and quantification of HaCaT cell migration ($n = 3$). Scale bars, 100 μm. (**H** and **I**) Representative images and quantitative analysis of transwell migration assay in HUVECs ($n = 3$). Scale bars, 200 μm. (**J** and **K**) Representative images and quantification of HUVECs' tube formation ($n = 3$). Scale bars, 200 μm. Significantly different (one-way ANOVA): *$P < 0.05$, **$P < 0.01$, and ***$P < 0.001$.

angiogenesis. The addition of alga-gel in the light significantly enhanced the migration of HUVECs and induced faster closure of the cell-free gap compared with the other groups (fig. S3), suggesting that dissolved oxygen released by PCC7942 enhanced the mobility of HUVECs (Fig. 2, H and I). Next, the results from Matrigel tube formation assay, which was carried out to evaluate vessel-forming capability, showed that tube length and branches assessed 6 hours later were significantly higher in the alga-gel (light)–treated HUVECs compared with TGO-treated HUVECs (Fig. 2, J and K). Collectively, these results indicated that enhanced vessel formation shown in a number of in vitro assays was due to the dissolved oxygen released from PCC7942, which is consistent with our next results in vivo.

We further speculated whether PCC7942 could elicit immune response. Macrophages usually represent a dominant proportion of the immune cell infiltrate and can be polarized to M1-like (NOS2 and IL12) including proinflammatory response (25). Our data confirmed that PCC7942 did not increase NOS2 and IL12 expression, compared to the control group, which validated no immune response with *Synechococcus* (fig. S4).

AGP transformed nonhealing chronic wound into acute wound-healing phenotype

We hypothesized that the enhanced cell proliferation and migration effects of PCC7942 in vitro will translate to an accelerated wound-healing response in vivo. Digital photographs of wounds showed that mice treated with alga-gel in the light exhibited much faster wound closure compared to the other groups (fig. S5, A and B), and even with 50% closure achieved at day 3 (fig. S5, C and D). These results indicate that PCC7942 is able to promote the wound healing by enhancing tissue oxygenation through photosynthesis.

To test the efficacy of AGP in healing chronic wounds, a diabetic mouse model was first established by feeding mice a high-fat and high-sugar diet and by streptozotocin (STZ) injection. Two weeks after the first STZ injection, treated mice with plasma glucose levels ≥16.7 mM were considered diabetic (26). A 10-mm-diameter full-thickness skin wound was then made on the dorsum of each mouse and fixed by stitching with a rubber ring to prevent natural skin contraction (27). Diabetic mouse wounds were treated by AGP (DM-AGP) and TGO therapy (DM-TGO) once a day, respectively. Diabetic mouse wounds (DM-Control) and normal mouse wounds (Non-DM) without treatment have also been evaluated as controls.

We observed that diabetic mouse wounds were difficult to heal even after 15 days, while wounds on normal mice can heal in 12 days (Fig. 3A). Wounds treated with AGP healed at a significantly faster rate than wounds treated with the TGO and diabetic control groups, with 45% closure achieved at day 6 relative to 20% for TGO and STZ groups (Fig. 3B). AGP outperformed other groups starting on day 6 after wounding, with 45% of the wound area closed by day 12, similar to normal mice (Fig. 3C).

Wounds were then assessed via histology at days 3, 6, 9, and 12 after wounding (fig. S6, A and C, and Fig. 3D). Wound re-epithelialization and granulation tissue formation were assessed histologically through measurements of the epithelial gap and granulation tissue thickness. Histology of the regenerated wounded tissue at day 12 revealed close to complete re-epithelialization in acute wounds, whereas DM-Control and TGO-treated wounds had remaining gaps of 2.15 ± 0.82 mm and 2.85 ± 1.08 mm, respectively (Fig. 3, F to H), while AGP-treated wounds had a multilayered epithelium structure that closely resembled healthy epidermis of the intact skin. The first prob-lem with chronic wounds is that they persist in the chronic inflammatory stage, while acute inflammation occurs in normal wounds for only a few days. Therefore, we determined the number of macrophages in tissues by CD68/CD31 immunostaining; AGP-treated wounds were also populated by vascular endothelial cells, which further supports the role of AGP in promoting angiogenesis during the healing process (Fig. 3, E and I). Consistent with the observations in murine macrophages, we observed that staining for the macrophage cell marker CD68 shows most macrophages in the DM-Control group, with the least amount within the AGP-treated tissue, suggesting a more subdued inflammatory status consistent with the control acute wound of a more advanced stage of the healing process (fig. S7).

We shortened the healing time of chronic wounds to the same time as that of normal wounds. This result leads us to doubt whether the use of AGP contributes to the healing of chronic wounds and, to some extent, to the transformation of chronic wounds into acute wounds. Gene expression exhibited significantly ($P < 0.05$) decreased levels in AGP-treated DM (DM-AGP) compared to nonhealing DM (DM), including members of the NF-κB and GSK-3β (PI3K-Akt pathway), the β-catenin (28), and HIF-1α and inducible nitric oxide synthase (iNOS). VEGFR1 (29) was elevated in AGP-treated DM, which was similar to the Non-DM and even the skin of normal mice (intact skin) (Fig. 3J). Under high-glucose conditions, HIF-1α proteins are stabilized and initiate the expression of multiple genes that are critical for angiogenesis, most notably the iNOS. In diabetes, the functional activity of HIF-1α is decreased, which results in a failure of the wound to up-regulate VEGFR1, leading to impaired angiogenesis and wound healing (11).

AGP promoted skin flap regeneration

Autograft microskin transplantation has been widely used as a skin graft therapy for wounds with massive skin deficits (30). However, skin grafting failure results in a pathological delay wound healing due to a poor vascularization wound bed (31).

To investigate whether AGP also played a positive role in promoting skin flap survival on chronic wounds, we assessed the effects of AGP on an autologous skin transplantation model in vivo. Skin flaps of about 1 cm (width) by 2 cm (length) were elevated on the back of diabetic and normal Balb/C mice with one short side connected (Fig. 4A) (32). Groups included normal mice control, diabetic mice control, and diabetic mice treated with TGO or AGP. Mice were anesthetized and photographed every 2 days; skin flaps on diabetic mice rapidly showed distal end necrosis at day 2 and then completely necrosed and dropped with the underlying ulcers exposed after day 4. Although normal mice were not affected by chronic wounds, the flaps still could not survive completely, and the distal part of the flaps appeared to be slightly necrotic after day 2 and dropped at day 6 (Fig. 4A). The average necrosis rates in Non-DM, DM-Control, and DM-TGO were 51.4%, 97.5%, and 58.0%, respectively, while the average necrosis rate in the AGP-treated group was 18% ($n = 6$). Lower skin flap necrosis rates were observed in DM-AGP even compared to normal mice (Fig. 4C). Consistent with H&E and Masson staining of the flap necrosis, we observed that the flap treated with AGP had intact epithelial structure, abundant granulation tissue, and a large number of collagen arranged neatly, which closely resembled healthy epidermis of the intact skin (fig. S8).

Both vascular network remodeling and blood skin flap survival rates were assessed by using a moorFLPI (Moor Instruments, UK)
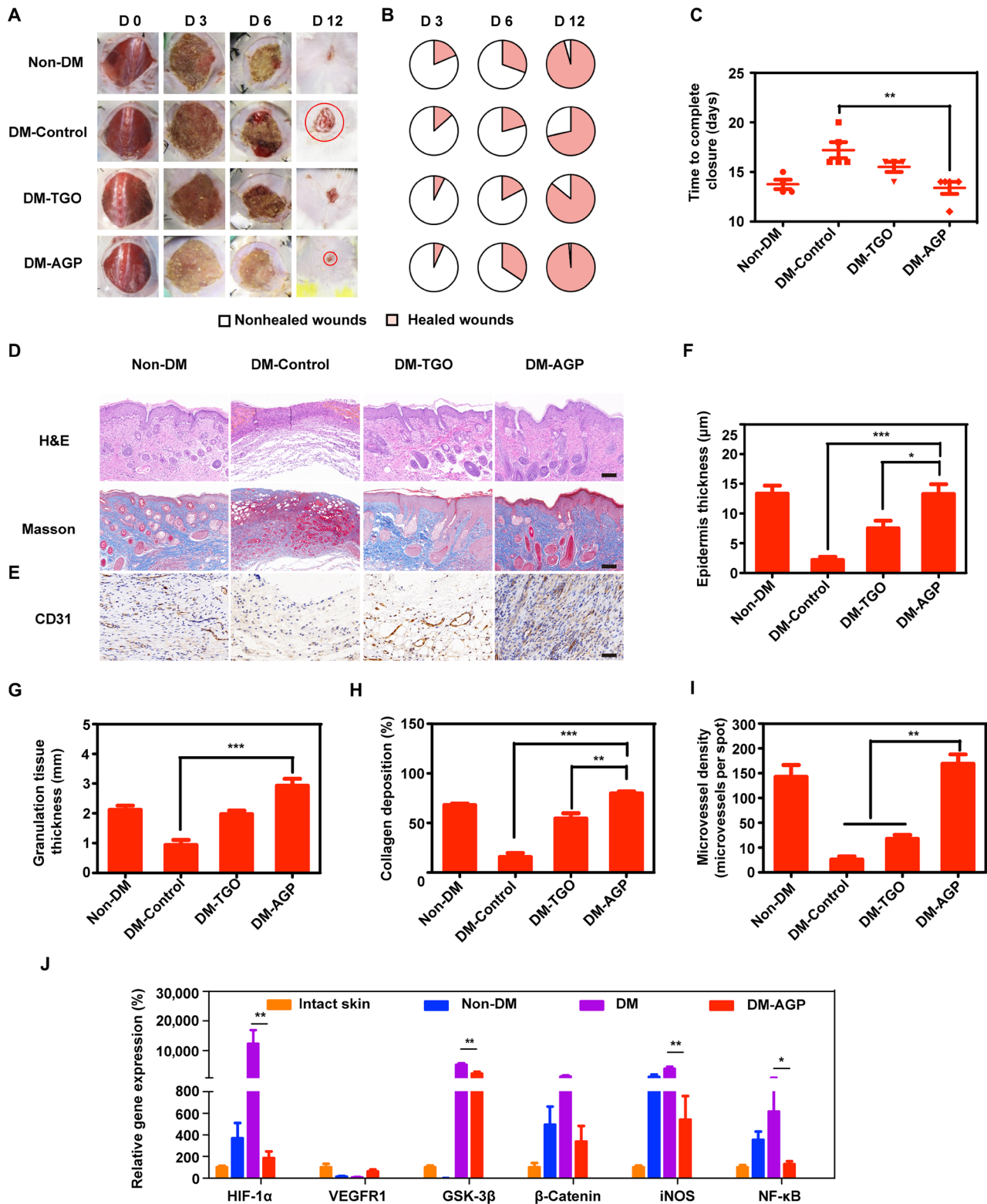
Fig. 3. AGP accelerated diabetic wounds by turning chronic into acute. (**A**) Representative images of the wound area by different treatments on days 0, 3, 6, and 12 after operation (*n* = 6). (**B**) Fractions of wounds healed by different treatments at days 3, 6, and 12 (*n* = 6). (**C**) Summary of the complete wound-closure times (*n* = 6). (**D**) H&E and Masson staining of the wound area reflected the regenerated skin in different groups at day 12 (*n* = 3). Scale bars, 100 μm. (**E**) Immunohistochemical images of the blood vessel CD31-positive endothelial cells (*n* = 3). Scale bar, 50 μm. Quantification of the epithelial gap (**F**), granulation tissue (**G**), and collagen deposition (**H**) in different groups (*n* = 3). (**I**) The average microvessel densities in different groups (*n* = 3). (**J**) Gene expression levels of quantitative PCR show that AGP accelerated diabetic wounds by turning chronic into acute (*n* = 3). Significantly different (one-way ANOVA): *$P < 0.05$, **$P < 0.01$, and ***$P < 0.001$. Photo credit (A): Huanhuan Chen (Medical School and School of Life Sciences, Nanjing University).
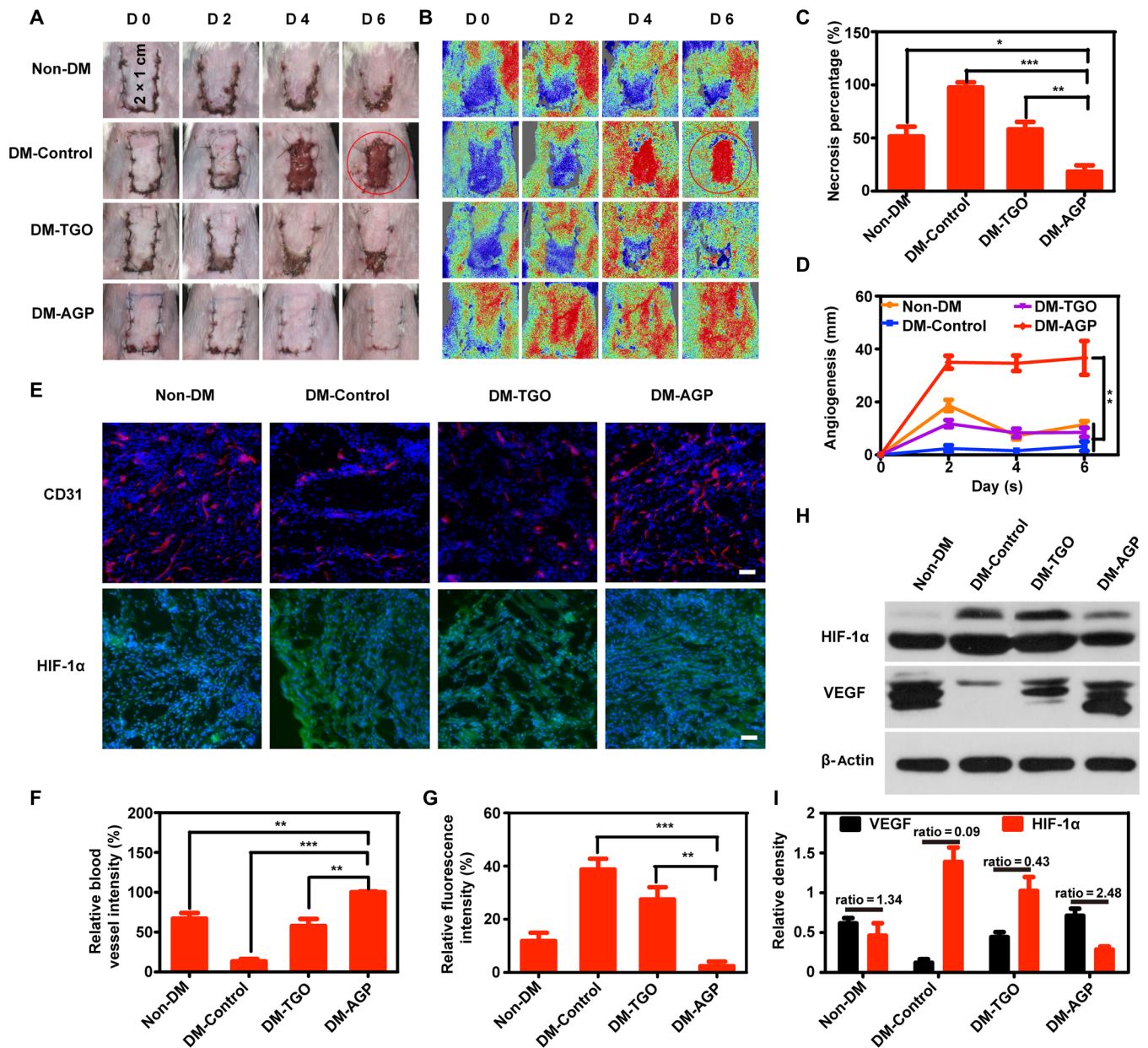
Fig. 4. AGP promotes skin flap regeneration and angiogenesis. (**A** and **B**) Photographic images of the skin flaps and the laser speckle contrast imaging captured real-time blood flow images from the Non-DM, DM-Control, DM-TGO, and DM-AGP groups 6 days after operation ($n = 7$). (**C**) Flap necrosis area percentages of different groups ($n = 6$). (**D**) Flap angiogenesis length of different groups ($n = 6$). (**E**) Immunofluorescence images of flaps highlighting blood vessel CD31-positive endothelial cells (red) and HIF-1α (green) ($n = 3$). Scale bars, 50 μm. (**F** and **G**) The average microvessel and HIF-1α densities in different groups ($n = 3$). (**H** and **I**) Western blotting data showing the levels of angiogenesis-related growth factors and hypoxia ($n = 3$). Significantly different (one-way ANOVA): *$P < 0.05$, **$P < 0.01$, and ***$P < 0.001$. Photo credit (A): Huanhuan Chen (Medical School and School of Life Sciences, Nanjing University).

imaging system to detect the real-time flap blood flow. The contrast images obtained were color-coded to correlate with the blood flow of the flap. In the circled areas in Non-DM, DM-Control, and DM-TGO groups, necrotic skin completely exfoliated and ulcerated, making the Doppler signal abruptly red. In the AGP treatment group, no necrotic skin was found, and grafts produced red color similar to normal skin (Fig. 4B). Recovered blood flow accompanied by wound closure ensures the long-term survival of skin flaps. Then, averaged lengths of closed incision with normalized blood flow signal were

measured. We found that the blood flow reconstruction speed of the drug group was the fastest. On day 6, the flap was completely closed, while the incision of the other group did not fully form the blood flow connection. Furthermore, the length of the reconstructed vessels was nearly 4 cm in AGP-treated mice, compared to the other groups (Fig. 4D). These results indicated the survival rate of flaps.

Immunohistochemical staining of CD31 and HIF-1α was performed to study the skin flap neovascularization. Cross sections of the flap revealed that AGP significantly increased the densities of the flap

microvessels. After 6 days, compared to the AGP group, the average microvessel densities were 66.9 ± 12.0%, 13.1 ± 5%, and 25.9 ± 9.9% in the Non-DM, DM, and TGO group, respectively (Fig. 4, E and F). Conversely, the HIF-1α staining in the AGP group was significantly lower than that in the DM and TGO groups, and even in the Non-DM group (Fig. 4E). The relative density was 2.3 ± 2% in the AGP group, while it was 11.8 ± 5% in the Non-DM group (Fig. 4G). The results showed that AGP could alleviate the mild local hypoxia by releasing dissolved oxygen.

The protein expression levels of VEGF and HIF-1α were identified by Western blot analysis (Fig. 4H). It is generally believed that high expression of HIF can stimulate high expression of VEGF, but a continuous hypoxia inhibits VEGF release (11). Because of the lack of oxygen, although the HIF-1α expressions of DM-Control and DM-AGP are higher than that of the Non-DM group, the VEGF expresses less than the Non-DM group. Moreover, as shown in Fig. 4I, the expression level of VEGF in the groups treated with AGP is much higher, and the ratio of VEGF to HIF-1α was 2.48. Pharmacological studies related to diabetic wound healing reported that neogenetic capillaries could improve microcirculation and provide oxygen and abundant nutrients for tissue repair around regions (14, 33). Our study found that PCC7942 characteristically might promote angiogenesis of diabetic skin ulcers.

DISCUSSION

This invention of AGPs points to producing continuous oxygen, which can effectively penetrate the skin, allowing for various hypoxic chronic wounds. By controllable photosynthesis of PCC7942, the moist environment is capable of gas absorption and permeation in wound tissue, for the further benefit of improving oxygen penetration to stimulate aerobic metabolism and angiogenesis in hypoxic tissues (34).

Another advantage worth mentioning is that both TDO and TGO can penetrate the hydrophilic PTFE membrane widely used in medicine, while bacteria are prevented from penetrating the wound surface. In addition, the manufacture of AGP is especially simple and low in cost (the cost of materials in our laboratory for a 9-cm^2 AGP is less than US$1). Also worth mentioning is the convenient and safe features of AGP, which paved a new strategy for conventional delivery of oxygen to DFU in large-animal models and clinical studies for the full transformation value of AGP. The establishment of a simulation-based approach here may also lead to the future design of AGP customization based on the patient's wound area and geometry, with the manufactured AGP meeting an individual's needs. It should also be noted that, apart from the TDO, our data suggested that PCC7942 may contain growth factors by promoting cell proliferation and migration in the absence of light, thus providing potential for promoting wound healing.

In conclusion, we demonstrate the potential feasibility of a novel concept for delivery of natural, highly reliable, moist oxygen to tissues, using tissue-adhesive microalgae hydrogel patches that have stable storage properties, and are easy to fabricate and handle. Considering that this approach can similarly be used in other treatments, such as cytokine therapy, noninvasive stem cell therapy, and drug delivery, our microalgal wound dressing could have diverse applications in translational and regenerative medicine, such as use in tissue and organ regeneration.

MATERIALS AND METHODS
O$_2$ release from PCC7942
The O$_2$ concentration measurements were acquired by the oxygen electrodes (OX-N-904151, Unisense). PCC7942 was obtained from

the Freshwater Algae Culture Collection at the Institute of Hydrobiology (FACHB-805; Chinese Academy of Sciences, Wuhan, China). The cyanobacteria were incubated in BG-11 liquid medium (GIBCO-BRL Life Technologies, Grand Island, USA) in 150-ml conical flasks. PCC7942 was collected by centrifugation at 8000 rpm for 5 min. The supernatants were removed and then the precipitates were repeatedly washed three times with phosphate-buffered saline (PBS) before they were redispersed in PBS. To determine the light response of PCC7942, PCC7942 (1×10^9 cells/ml) solution was added into a penicillin bottle and exposed to a 620- to 660-nm near-infrared light-emitting diode (NIR LED) at 0.5 W/cm^2 power density for 30 min and then stored under dark conditions for 30 min in a 6-cycle period. To verify whether carbon sources can increase the oxygen production of PCC7942, PCC7942 (1×10^9 cells/ml) was resuspended in PBS supplement with 125, 250, and 500 μM Na$_2$CO$_3$ and then exposed to the NIR LED for 30 min.

Preparation and O$_2$ production of alga-gel
Sodium alginate (8%) was added into the PCC7942 solution (with 500 μM Na$_2$CO$_3$). Subsequently, the solution was dripped into 3% calcium chloride using a 1-ml syringe on the magnetic stirrer to make the uniform-sized alga-gel particle (35). To compare the O$_2$ production of alga-gel with PCC7942 (1×10^9 cells/ml), we put alga-gel in PBS with or without 500 μM Na$_2$CO$_3$ and tested the oxygen generation by the microelectrode under light conditions.

Preparation of AGP
The alga-gel was encapsulated by a sterile and 0.22-μm porous polytetrafluoroethylene membrane as inner lining (36) and a transparent polyurethane film as back lining to manufacture AGP.

Dissolved oxygen of AGP penetrates skin
The objective was to determine the rate at which oxygen was transferred from AGP or TGO to physiologic saline through the test apparatus. The apparatus consists of a 10-ml chamber containing physiological saline in a closed system with a 3 cm by 3 cm mesh to which mice skin samples adhered (Fig. 1G). The instrument was filled with physiological saline in an aqueous environment with nearly no oxygen at first and maintained at 37°C. To determine the baseline transfer kinetics of oxygen delivery, the external AGP exposed to a 620- to 660-nm NIR LED was placed on the mesh and recorded. To determine the effect of TGO, medical grade 100% oxygen was applied with a continuous flow rate of 5 liters/min with a silica gel collapsible bulb. To determine whether dissolved oxygen or TGO penetrated the skin, three mouse skin samples (300 to 400 μm) excised from the back were obtained and fixed over the mesh of the test apparatus, and then the external AGP or 100% TGO was applied.

Stability studies of AGP
PCC7942 solution, alga-gel, and AGP were dispersed in BG11 (pH 7.4) at 4°C in the dark for 3, 6, 9, 12, and 15 days. The amount of O$_2$ release and photographs of alga-gel solutions were monitored to evaluate the stability of alga-gel at different time points.

Cell culture
HUVECs, HaCaTs, and HSFs were kindly obtained from Nanjing University School of Medicine. HUVECs and HaCaTs were incubated in RPMI 1640 medium (Gibco) containing 10% fetal bovine serum (FBS; Gibco). HSFs were cultured in high-glucose Dulbecco's modified

Eagle's medium (DMEM; Gibco) supplemented with 10% FBS in the incubator at 37°C and 5% CO2.

Immunofluorescence for HIF-1α expression in vitro

To evaluate the ability of algal-gel to promote wound healing, we performed in vitro simulations of these three cells. HUVECs, HaCaTs, and HSF cells were plated at a density of 5×10^4 cells per well into the lower chamber of 24-well transwell inserts with 8-μm pore-sized filters (Corning, NY, USA). The control group was cultured in basal medium; other groups grown for high-glucose concentrations (33 mM) were exposed for an additional 6 hours to hypoxia (1% O_2), as specified hypoxia. Then, the gaseous-oxygen group was treated with medical grade 100% oxygen at 1.5 atm for 3 hours, while the alga-gel group was treated with alga-gel (1×10^9 cells/ml) into the upper chamber with NIR LED for 1 hour, followed by the use of an illumination incubator. After 24 hours, cells were fixed with 4% paraformaldehyde (PFA) for 15 min, the cell membrane was ruptured with 0.3% Triton X-100 for 30 min, and then cells were blocked with 5% bovine serum albumin (BSA) blocking solution for 30 min. To evaluate the hypoxia, all of the three types of cells were incubated with the primary antibody HIF-1α (Cell Signaling, 36169) at room temperature for 30 min and then incubated with second antibody anti-rabbit immunoglobulin G (IgG) (Cell Signaling, 4412S) at room temperature in the dark for 30 min. After washing with PBS, 4′,6-diamidino-2-phenylindole (DAPI) (Sigma-Aldrich) was used to stain nuclei for 10 min. Cells were imaged under a confocal laser scanning microscope (FV1000, Olympus, Japan) and quantified using ImageJ software. To assess cell viability, HSF and HUVECs were stained with Calcein-AM.

Scratch wound-healing assay

Cell scratch was measured using 24-well transwell inserts with 8-μm pore-sized filters. Briefly, cells were subcultured at a density of 1×10^5 cells per well into the lower chamber and scratched using a sterile p200 pipette tip and washed with PBS to remove unattached cells. Then, the attached cells were treated with alga-gel (1×10^9 cells/ml) into the upper chamber in the light or TGO. HaCaTs and HUVECs were photographed at 0, 12, and 24 hours after wounding. The migration rate was evaluated by calculating the ratio of the closed area to the initial wound.

Transwell migration assay

For cell migration assay, HUVECs were seeded into the upper chamber with a density of 1×10^4 cells per well (37); the lower chamber was added with alga-gel (1×10^9 cells/ml) or treated with TGO. After 24 hours, the migrated cells kept on the upper surface filter were removed by cotton swab, while the migrated cells on the bottom side of the filter were stained with a 0.5% crystal violet solution for 1 hour. The number of migrated cells was photographed and counted under an optical microscope (Nikon, Japan).

Tube formation assay

For tube formation assay, 250 μl per well of thawed Matrigel (BD, USA) was added into the lower chamber of a pre-cooled 24-well plate and incubated for 1 hour at 37°C (38). Then, HUVECs were seeded with 5×10^4 cells per well into the Matrigel-coated lower chamber and exposed to alga-gel (1×10^9 cells/ml) into the upper chamber in the light or TGO for 6 hours. To assess the tube formation, HUVECs, stained with Calcein-AM, were imaged under a confocal laser scanning microscope and quantified using ImageJ software.

In vitro immune response

For transcriptional analysis of murine macrophages, RAW264.7 cells were seeded into the lower chamber of a 24-well transwell with a density of 5×10^4 cells per well, and the upper chamber was added with alga-gel (1×10^9 cells/ml). After 24 hours, RNA was extracted using TRIzol reagent (Invitrogen) and subjected to reverse transcription with a RevertAid First Strand cDNA Synthesis Kit (Fermentas, Burlington, Canada). The relative gene expression of NOS2 and IL12 was calculated and glyceraldehyde-3-phosphate dehydrogenase (GAPDH) was used as an internal control gene to normalize the expression of the target gene. Primer sequences used for quantitative real-time polymerase chain reaction (qRT-PCR) analysis were as follows: NOS2: forward, 5′-CAAGCTGAACTTGAGCGAGGA-3′, and reverse, 5′-TTTACTCAGTGCCAGAAGCTGGA-3′; IL12: forward, 5′-TGACACGCCTGAAGAAGATGAC-3′, and reverse, 5′-ACT-GCTACTGCTCTTGATGTTGAAC-3′; GAPDH: forward, 5′-TCCCG-TAGACAAAATGGTGAAGG-3′, and reverse, 5′-ATGTTAGTG-GGGTCTCGCTCCTG-3′.

Animals

Balb/C mice (male, about 25 g in weight) and high-fat and high-sugar feed were obtained from Yangzhou University Medical Centre (Yangzhou, China). Balb/C mice (in groups of six) had free access to abundant food and water. All animal operations and experimental procedures were approved by the Administration Committee of Experimental Animals in Jiangsu Province and the Ethics Committee of Nanjing University.

Acute wound-healing mice

A full-thickness wound was made on the center of dorsum of Balb/C mice to remove the epidermis and superficial parts of the dermis by using a 5-mm biopsy punch. The animals were randomly divided into five groups: a control group, a PU film group, a gel group without PCC7942, an AGP (light) group containing 1×10^9/ml PCC7942 exposed to a 620- to 660-nm NIR LED for 60 min, and an AGP group containing 1×10^9 ml of PCC7942 with dark treatment. Freshly prepared AGP (light), AGP (dark), gel, or PU film was covered on the wound topically every day, while the control wounds were left exposed to air. The wound area was measured and captured with a digital camera on the day of surgery, day 2, and every 2 days until the wound was completely healed.

STZ-induced diabetic models

Balb/C male mice were fed with high-fat and high-sugar feed and maintained under specific pathogen–free environment. Briefly, the animals other than those in the control group ($n = 10$) were administered STZ (100 mg/kg; Sigma-Aldrich) mixed in sodium citrate buffer (intraperitoneal injection) daily for two consecutive days. All of the treated mice with plasma glucose levels ≥16.7 mM under normal condition were considered diabetic 2 weeks after the first STZ injection (26). Animals were maintained in a diabetic state for the wound healing and skin flap regeneration experiment.

Chronic wound-healing mice

The STZ-induced diabetic mice were anesthetized under sterile conditions, and then a full-thickness wound was made on the center of dorsum to remove the epidermis and superficial parts of the dermis by using a 10-mm biopsy punch. The animals were randomly divided into four groups: control group, STZ group, STZ

with TGO group as the clinical treatment, and STZ with AGP group containing 1×10^9 ml of PCC7942 exposed to a 620- to 660-nm NIR LED for 60 min. Pure oxygen was applied for the TGO group mice at 1.03 atm for 90 min with a catheter on the wound every day (*39*). The fresh AGP was covered with AGP group every day. Digital images of the wound area were captured on the day of surgery and every other day after wounding. A ruler reference was placed nearby to correct the distance between the animals and the camera. The wound area was quantified by three blinded observers using ImageJ software [Version 1.32; National Institutes of Health (NIH)], corrected the area of the reference circle, and expressed as a percentage of the original area. The animals were randomly selected and euthanized on day 3 (inflammation stage), day 6 (proliferation stage), and day 12 (maturation stage) after surgery (*40*). Harvested wound tissues were either fixed in 4% PFA in PBS, or flash-frozen in liquid nitrogen, and used for further immunohistological and immunofluorescence investigations and mRNA expression analysis.

Skin flap regeneration mice
The STZ-induced diabetic mice were anesthetized under sterile conditions, and then a 2-cm (length) by 1-cm (width) flap area was marked on the back of mice. The subcutaneous soft tissue was completely disconnected by evaluating the full-thickness flap and then the flap was carefully sutured back to its original position. The mice were randomly divided into four groups: control group, STZ group, STZ with TOT group as the clinical treatment, and STZ with AGP group containing 1×10^9 ml of PCC7942 exposed to a 620- to 660-nm NIR LED for 60 min. In the TGO treatment group, mice received 100% oxygen at 1.03 atm for 30 min with a catheter on the transplanted flap every day. Freshly prepared AGP was covered on the flap of the AGP group every day. All the mice were anesthetized, and the surviving and necrotic areas of the flaps were photographed using a digital camera every other day after surgery. Meanwhile, the necrosis rates were assessed using the moorFLPI (Moor Instruments, UK) to detect the real-time flap blood flow. The contrast images were monitored using the laser speckle contrast technique. The necrotic areas were quantified by using ImageJ software (Version 1.32; NIH) as the percentage of the original flap areas, and the length of the reconstructed blood vessels was considered as the percentage of the initial disconnected blood vessel. The data analysis was blinded. The purpose of this experiment was to analyze histology and immunofluorescence and protein expression during the skin flap regeneration; the animals were killed on day 6 after surgery when the flap was totally transplanted back. Each 1 cm by 0.5 cm similar position of the surviving and necrotic flap area junction was harvested. Subsequently, one flap tissue was fixed in 4% PFA in PBS, while the other was snap-frozen in liquid nitrogen.

Histology and Immunohistochemistry
Immunohistochemical analysis of CD31 and CD68: 5-µm-thick paraffin-embedded tissue was performed for immunohistochemical analysis. Briefly, after dewaxing and quenching the endogenous peroxidase activity with 3% H_2O_2 for 10 min, the section was rinsed with PBS and blocked in 5% BSA for 10 min. The slice was incubated with the primary antibody (mouse anti-CD31 antibody, 1:100; Abcam, USA; mouse anti-CD68 antibody, 1:100; Abcam, USA) at 4°C overnight and then added with horseradish peroxidase (HRP)–conjugated secondary goat anti-rat antibody at room

temperature for 30 min. The sections were observed and photographed using a microscope connected to a digital camera.

Immunofluorescence staining
All tissue sections were embedded into optimal cutting temperature (OCT) compound and cryosectioned into 8-µm-thick frozen sections in liquid nitrogen for fluorescent immunostaining. After deparaffinization by ice-cold acetone, the slice was rinsed in PBS and then blocked with 5% of BSA blocking solution for 1 hour. To evaluate the blood vessels and hypoxia, the slices were incubated with the antibody CD31 (BioLegend, 102408) and HIF-1α (Cell Signaling, 36169) at 4°C overnight; after washing several times with PBS, DAPI (Sigma-Aldrich) was used to stain nuclei for 10 min. The sections were imaged with a fluorescence microscope. Five to 10 immunofluorescence images per marker were randomly collected and quantified using ImageJ software.

qRT-PCR analysis in vivo
The RNA of the skin sections was extracted using TRIzol reagent (Invitrogen) according to the manufacturer's protocol. Complementary DNA (cDNA) was obtained by reverse-transcribing total RNA with a RevertAid First Strand cDNA Synthesis Kit (Fermentas, Burlington, Canada) performed on an ABI PRISM 7900HT System (Applied Biosystems) using SYBR Green Master Mix (Thermo Fisher Scientific). The $2^{-\Delta\Delta Ct}$ method was used to calculate the relative gene expression, and β-actin was used as an internal control gene to normalize the expression of the target gene. Primer sequences used for qRT-PCR analysis were as follows: VEGFR1: forward, 5′-GAAAC-CACAGCAGGAAGACG-3′, and reverse, 5′-CTTTATGCCCAG-CAAGATCG-3′; HIF-1α: forward, 5′-CTATGGAGGCCAGAA-GAGGGTAT-3′, and reverse, 5′-CCCACATCAGGTGGCTCATAA-3′; iNOS: forward, 5′-CTCACCTACTTCTGGACATTAC-3′, and reverse, 5′-GCCTCCAATCTCTGCCTATC-3′; GSK-3β: forward, 5′-GGT-GAATCGAGAAGAGCCA-3′, and reverse, 5′-CTCCTGAGTCA-CAAAGTTTG-3′; β-catenin: forward, 5′-GGCCATTGTAGAAGCT-GGTG-3′, and reverse, 5′-CTGCTTAGTCGCTGCATCTG-3′; NF-kB: forward, 5′-TCTCTATGACCTGGACGACTCTT-3′, and reverse, 5′-GCTCATACGGTTTCCCATTTAGT-3′; β-actin: forward, 5′-TCAG-GTCATCACTATCGGCAAT-3′, and reverse, 5′-AAAGAAAGG-GTGTAAAACGCA-3′.

Western blotting
Western blot analysis of HIF1-α and VEGF: Skin flap tissues were homogenized in Laemmli sample buffer and determined using the bicinchoninic acid protein assay for protein content. Then, 20 µg of total protein was separated by 10% SDS-polyacrylamide gel electrophoresis (SDS-PAGE) and transferred to polyvinylidene difluoride membranes (Millipore) by electroblotting. After washing with tris-buffered saline solution in 0.1% Tween-20 (Merck) (TBS-T), the members were blocked in 5% w/v fat-free milk powder (Roth) for 1 hour at room temperature and then washed with TBST. The members were incubated with primary antibody: HIF1-α (Cell Signaling), VEGF (Cell Signaling), and rabbit antihuman β-actin (Cell Signaling) overnight at 4°C. After washing, the members were incubated with an HRP-labeled secondary antibody (goat anti-rabbit IgG; Cell Signaling) for 1 hour at room temperature. Bound antibodies' images were developed by ECL reagent (ECL Advance Western Blotting Detection Kit, GE Healthcare) in the dark and detected using a fluorescence imaging analysis system. The protein expression was quantified by ImageJ software (NIH).

Statistical analysis

Statistical significance was determined using unpaired and paired two-sided Student's t tests as indicated; data are presented as single measurements with bars as group means ± SD. For histochemical analysis, a one-way analysis of variance (ANOVA) with Holm–Sidak's multiple comparisons was used to determine statistical significance; data are means ± SD; $P < 0.05$ was considered significant.

SUPPLEMENTARY MATERIALS

Supplementary material for this article is available at http://advances.sciencemag.org/cgi/content/full/6/20/eaba4311/DC1

View/request a protocol for this paper from *Bio-protocol*.

REFERENCES AND NOTES

1. International Diabetes Federation, *IDF Diabetes Atlas* (IDF, ed. 8, 2017).
2. T. Hart, R. Milner, A. Cifu, Management of a diabetic foot. *JAMA* **318**, 1387–1388 (2017).
3. I. R. Botusan, V. G. Sunkari, O. Savu, A. I. Catrina, J. Grünler, S. Lindberg, T. Pereira, S. Ylä-Herttuala, L. Poellinger, K. Brismar, S. B. Catrina, Stabilization of HIF-1α is critical to improve wound healing in diabetic mice. *Proc. Natl. Acad. Sci. U.S.A.* **105**, 19426–19431 (2008).
4. H. Thangarajah, I. N. Vial, R. H. Grogan, D. Yao, Y. Shi, M. Januszyk, R. D. Galiano, E. I. Chang, M. G. Galvez, J. P. Glotzbach, V. W. Wong, M. Brownlee, G. C. Gurtner, HIF-1α dysfunction in diabetes. *Cell Cycle* **9**, 75–79 (2010).
5. Y. D. Thangarajah, D. Yao, E. I. Chang, Y. Shi, L. Jazayeri, I. N. Vial, R. D. Galiano, X. L. Du, R. Grogan, M. G. Galvez, M. Januszyk, M. Brownlee, G. C. Gurtner, The molecular basis for impaired hypoxia-induced VEGF expression in diabetic tissues. *Proc. Natl. Acad. Sci. U.S.A.* **106**, 13505–13510 (2009).
6. Y. Zhu, Y. Wang, Y. Jia, J. Xu, Y. Chai, Roxadustat promotes angiogenesis through HIF-1α/VEGF/VEGFR2 signaling and accelerates cutaneous wound healing in diabetic rats. *Wound Repair Regen.* **27**, 324–334 (2019).
7. M. Heyboer III, D. Sharma, W. Santiago, N. McCulloch, Hyperbaric oxygen therapy: Side effects defined and quantified. *Adv. Wound Care* **6**, 210–224 (2017).
8. P. Kranke, M. Bennett, I. Roeckl-Wiedmann, S. Debus, Hyperbaric oxygen therapy for chronic wounds. *Cochrane Database Syst. Rev.* **2004**, CD004123 (2015).
9. C. Y. Chen, R. W. Wu, M. C. Hsu, C. J. Hsieh, M. C. Chou, Adjunctive hyperbaric oxygen therapy for healing of chronic diabetic foot ulcers. *J. Wound Ostomy Continence Nurs.* **44**, 536–545 (2017).
10. S. Opasanon, W. Pongsapich, S. Taweepraditpol, B. Suktitipat, A. Chuangsuwanich, Clinical effectiveness of hyperbaric oxygen therapy in complex wounds. *J. Am. Coll. Clin. Wound Spec.* **6**, 9–13 (2014).
11. H. W. Hopf, J. J. Gibson, A. P. Angeles, J. S. Constant, J. J. Feng, M. D. Rollins, M. Zamirul Hussain, T. K. Hunt, Hyperoxia and angiogenesis. *Wound Repair Regen.* **13**, 558–564 (2005).
12. A. Hodges, S. Delaney, J. Lecomte, V. Lacroix, D. Montgomery, Effect of hyperbaric oxygen on oxygen uptake and measurements in the blood and tissues in a normobaric environment. *Br. J. Sports Med.* **37**, 516–520 (2003).
13. D. F. Roe, B. L. Gibbins, D. A. Ladizinsky, Topical dissolved oxygen penetrates skin: Model and method. *J. Surg. Res.* **159**, e29–e36 (2010).
14. I. E. Gabbay, M. Gabbay, U. Gabbay, Diabetic foot cellular hypoxia may be due to capillary shunting—A novel hypothesis. *Med. Hypotheses* **82**, 57–59 (2014).
15. J. Espinosa, J. S. Boyd, R. Cantos, P. Salinas, S. S. Golden, A. Contreras, Cross-talk and regulatory interactions between the essential response regulator RpaB and cyanobacterial circadian clock output. *Proc. Natl. Acad. Sci. U.S.A.* **112**, 2198–2203 (2015).
16. Circadian rhythms in rapidly dividing cyanobacteria. *Science* **275**, 224–227 (1997).
17. C. A. Davis, Topical oxygen emulsion: A novel wound therapy. *Arch. Dermatol.* **143**, 1252–1256 (2007).
18. S. A. Reading, M. Yeomans, C. Levesque, Skin oxygen tension is improved by immersion in oxygen-enriched water. *Int. J. Cosmet. Sci.* **35**, 600–607 (2013).
19. J. Li, Y. P. Zhang, M. Zarei, L. Zhu, J. O. Sierra, P. M. Mertz, S. C. Davis, A topical aqueous oxygen emulsion stimulates granulation tissue formation in a porcine second-degree burn wound. *Burns* **41**, 1049–1057 (2015).
20. I. Moen, H. Ugland, N. Strömberg, E. Sjöström, A. Karlson, L. Ringstad, H. Bysell, M. Amiry-Moghaddam, C. Haglerød, Development of a novel in situ gelling skin dressing: Delivering high levels of dissolved oxygen at pH 5.5. *Health Sci. Rep.* **1**, e57 (2018).
21. S. Zellner, R. Manabat, D. F. Roe, A dissolved oxygen dressing: A pilot study in an ischemic skin flap model. *J. Int. Med. Res.* **43**, 93–103 (2015).
22. X. Zheng, S. Narayanan, V. G. Sunkari, S. Eliasson, I. R. Botusan, J. Grünler, A. I. Catrina, F. Radtke, C. Xu, A. Zhao, N. R. Ekberg, U. Lendahl, S. B. Catrina, Triggering of a Dll4-Notch1 loop impairs wound healing in diabetes. *Proc. Natl. Acad. Sci. U.S.A.* **116**, 6985–6994 (2019).
23. J. Yan, Z. Zhang, H. Shi, HIF-1 is involved in high glucose-induced paracellular permeability of brain endothelial cells. *Cell. Mol. Life Sci.* **69**, 115–128 (2012).
24. C. Liu, X. Cui, T. M. Ackermann, V. Flamini, W. Chen, A. B. Castillo, Osteoblast-derived paracrine factors regulate angiogenesis in response to mechanical stimulation. *Integr. Biol.* **8**, 785–794 (2016).
25. C. B. Rodell, S. P. Arlauckas, M. F. Cuccarese, C. S. Garris, R. Li, M. S. Ahmed, R. H. Kohler, M. J. Pittet, R. Weissleder, TLR7/8-agonist-loaded nanoparticles promote the polarization of tumour-associated macrophages to enhance cancer immunotherapy. *Nat. Biomed. Eng.* **2**, 578–588 (2018).
26. E. Vågesjö, E. Öhnstedt, A. Mortier, H. Lofton, F. Huss, P. Proost, S. Roos, M. Phillipson, Accelerated wound healing in mice by on-site production and delivery of CXCL12 by transformed lactic acid bacteria. *Proc. Natl. Acad. Sci. U.S.A.* **115**, 1895–1900 (2018).
27. J. Michaels, S. S. Churgin, K. M. Blechman, M. R. Greives, S. Aarabi, R. D. Galiano, G. C. Gurtner, db/dbmice exhibit severe wound-healing impairments compared with other murine diabetic strains in a silicone-splinted excisional wound model. *Wound Repair Regen.* **15**, 665–670 (2007).
28. R. C. Stone, O. Stojadinovic, A. M. Rosa, H. A. Ramirez, E. Badiavas, M. Blumenberg, M. Tomic-Canic, A bioengineered living cell construct activates an acute wound healing response in venous leg ulcers. *Sci. Transl. Med.* **9**, eaaf8611 (2017).
29. J. Zhou, M. Ni, X. Liu, Z. Ren, Z. Zheng, Curcumol promotes vascular endothelial growth factor (VEGF)–mediated diabetic wound healing in streptozotocin-induced hyperglycemic rats. *Med. Sci. Monit.* **23**, 555–562 (2017).
30. Y. Luo, X. Yi, T. Liang, S. Jiang, R. He, Y. Hu, L. Bai, C. Wang, K. Wang, L. Zhu, Autograft microskin combined with adipose-derived stem cell enhances wound healing in a full-thickness skin defect mouse model. *Stem Cell Res. Ther.* **10**, 279 (2019).
31. K. Y. Howangyin, J. S. Silvestre, Diabetes mellitus and ischemic diseases: Molecular mechanisms of vascular repair dysfunction. *Arterioscler. Thromb. Vasc. Biol.* **34**, 1126–1135 (2014).
32. X. Mao, C. Ruoyu, Z. Hongbo, B. Jinhong, C. Liying, Z. Lu, D. Lianfu, C. Wenguo, Z. Yuguang, H. A. Santos, S. Xiaoming, Self-healing and injectable hydrogel for matching skin flap regeneration. *Adv. Sci.* **6**, 1801555 (2019).
33. T. Dinh, A. Veves, Microcirculation of the diabetic foot. *Curr. Pharm. Des.* **11**, 2301–2309 (2005).
34. G. D. Winter, Formation of the scab and the rate of epithelization of superficial wounds in the skin of the young domestic pig. *Nature* **193**, 293–294 (1962).
35. M. Shi, H. Zhang, T. Song, X. Liu, Y. Gao, J. Zhou, Y. Li, Sustainable dual release of antibiotic and growth factor from pH-responsive uniform alginate composite microparticles to enhance wound healing. *ACS Appl. Mater. Interfaces* **11**, 22730–22744 (2019).
36. M. Du, H. Gong, H. Pang, Q. Shen, Z. Chen, Fabrication and characterization of poly(vinylidene fluoride)–polytetrafluoroethylene composite membrane for CO_2 absorption in gas–liquid contacting process. *J. Appl. Polym. Sci.* **136**, 47767 (2019).
37. H. Yin, C. Y. Chen, Y. W. Liu, Y. J. Tan, Z. L. Deng, F. Yang, F. Y. Huang, C. Wen, S. S. Rao, M. J. Luo, X. K. Hu, Z. Z. Liu, Z. X. Wang, J. Cao, H. M. Liu, J. H. Liu, T. Yue, S. Y. Tang, H. Xie, *Synechococcus elongatus* PCC7942 secretes extracellular vesicles to accelerate cutaneous wound healing by promoting angiogenesis. *Theranostics* **9**, 2678–2693 (2019).
38. S.-J. Park, R. Y. Kim, B.-W. Park, S. Lee, S. W. Choi, J.-H. Park, J. J. Choi, S.-W. Kim, J. Jang, D.-W. Cho, H.-M. Chung, S.-H. Moon, K. Ban, H.-J. Park, Dual stem cell therapy synergistically improves cardiac function and vascular regeneration following myocardial infarction. *Nat. Commun.* **10**, 3123 (2019).
39. K. Copeland, A. R. Purvis, A retrospective chart review of chronic wound patients treated with topical oxygen therapy. *Adv. Wound Care* **6**, 143–152 (2017).
40. H. S. Kim, X. Sun, J. H. Lee, H. W. Kim, X. Fu, K. W. Leong, Advanced drug delivery systems and artificial skin grafts for skin wound healing. *Adv. Drug Deliv. Rev.*, (2018).